Inorganic Chemistry

pubs.acs.org/IC Article

Macrocyclic Chromium(III) Catecholate Complexes

Ashley J. Schuman, Adharsh Raghavan, Susannah D. Banziger, You Song, Zhao-Bo Hu, Brandon L. Mash, Andrew L. Williams, and Tong Ren*

Cite This: *Inorg. Chem.* 2021, 60, 4447−4455 Read Online

ACCESS | Metrics & More | Article Recommendations | Supporting Information

ABSTRACT: The synthesis and structural, electrochemical, spectroscopic, and magnetic characterizations of Cr^{III}(HMC) catecholate and semiquinonate complexes are reported herein, where HMC is 5,5,7,12,12,14-hexamethyl-1,4,8,11-tetraazacyclotetradecane. *cis*-[Cr(HMC)(Cat)]$^+$ complexes (Cat = catecholate, [**1**]$^+$; tetrachlorocatecholate, [**2**]$^+$; and 3,5-di-*tert*-butylcatecholate, [**3**]$^+$) were prepared from the reaction between appropriate catechol and [Cr^{III}(HMC)Cl_2]Cl reduced *in situ* by zinc. Chemical oxidation of [**3**]$^+$ by $FcPF_6$ resulted in *cis*-[Cr(HMC)(SQ)]$^{2+}$ ([**3**]$^{2+}$, SQ = 3,5-di-*tert*-butylsemiquinonate). Single crystal X-ray diffraction studies revealed the *cis*-chelation of the Cat/SQ ligand around the Cr metal center and confirmed the Cat/SQ nature of the ligands. Reversible oxidations of Cat to SQ were observed in the cyclic voltammograms of [**1**]$^+$−[**3**]$^+$, while the Cr^{III} center remains redox inactive. The absorption spectrum of the SQ complex [**3**]$^{2+}$ exhibits an intense spin-forbidden transition in solution. Time-delayed phosphorescence spectra recorded at 77 K revealed that all catecholate complexes emit from the ^2E state, while [**2**]$^+$ also emits from the $^2T_1$ state. Temperature-dependent magnetic susceptibility measurements indicate the Cat complexes exist as $S = 3/2$ systems, while the SQ complex behaves as an $S = 1$ system, resulting from strong antiferromagnetic coupling of the $S = 3/2$ Cr center with the $S = 1/2$ SQ radical. Density functional theory (DFT) shows the similarities between the SOMOs of [**1**]$^+$ and [**2**]$^+$ and differences in their LUMOs in the ground state.

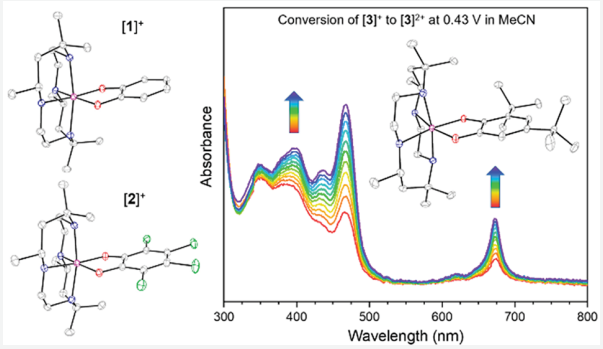

INTRODUCTION

Redox-active ligands have been of recent interest due to their ability to serve as an electron reservoir for transition metal catalysts.[1,2] Catecholate and its derivatives are the classic example of such ligands, which may exist in three valence states depending on the coordination environment: catecholate (Cat), semiquinonate (SQ), and benzoquinone (BQ) (Scheme 1).[3,4] Cat and SQ are known to readily coordinate to 3d transition metals, while BQ complexes remain elusive in the literature.[5] Cat/SQ complexes containing Mn, Fe, and Cu have been examined for various biological applications,[6] especially modeling the chemistry of catechol dioxygenases.[7−9] Co Cat/SQ complexes exhibit valence tautomerism,[10,11] making them a strong candidate for molecular switches and spin-crossover materials.[12,13] Metal−organic frameworks bridged by chloranilate (dianion of 3,6-dichloro-2,5-dihydroxy-1,4-benzoquinone) exhibited exceptionally high magnetic ordering temperature (M = Fe)[14] and expedient metal transport (M = Mn).[15]

Scheme 1. Oxidation States of Orthoquinones

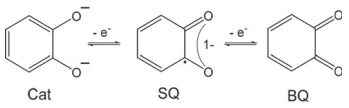

Metal−Cat/SQ complexes supported by an ancillary ligand (L) can be found throughout the literature. Paramagnetic metal−semiquinone systems are of interest because they contain only two components with unpaired spin, enabling the study of exchange coupling effects on electronic and photochemical properties. The photophysical properties of chromium(III) complexes are well established in the absence of electron exchange,[16−18] making chromium(III) Cat/SQ complexes ideal candidates for further study. The Cat/SQ ligand allows for exchange coupling to be turned on (SQ) or off (Cat) based on the oxidation state of the ligand, without altering the composition of the complex ion. Variation of the steric and electronic structure of L enables further tuning of M−Cat interactions in *cis*-[M(L)Cat)]$^+$ complexes.[3,4] Dei and co-workers have investigated a number of catecholate metal complexes supported by HMC (5,5,7,12,12,14-hexamethyl-1,4,8,11-tetraazacyclotetradecane, abbreviated as "CTH" by

Received: October 30, 2020
Published: March 12, 2021

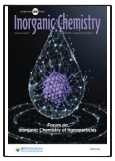

https://dx.doi.org/10.1021/acs.inorgchem.0c03224
Inorg. Chem. 2021, 60, 4447−4455

Scheme 2. Synthesis of *cis*-Cr^{III}(HMC) Catecholate Complexes; $[1]^+$ = $[Cr^{III}(HMC)(Cat)]^+$, $[2]^+$ = $[Cr^{III}(HMC)(L2)]^+$, and $[3]^+$ = $[Cr^{III}(HMC)(L3)]^+$

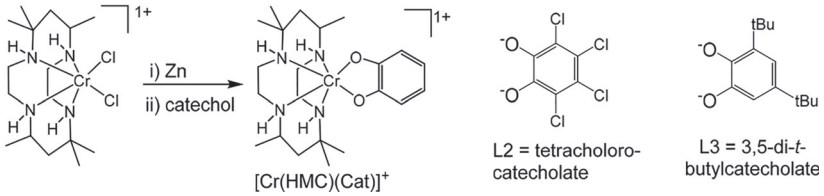

Dei) with metal center as Mn,[19,20] Fe,[20,21] Co,[22,23] Ni,[20,24−27] and Rh.[25] Especially relevant to this work, $Cr^{II}(HMC)Cl_2$ reacted with 3,5-di-*tert*-butylbenzoquinone (DTBBQ) or tetrachlorobenzoquinone (TCBQ) to afford the semiquinonate complex $[Cr^{III}(HMC)(DTBSQ)]^{2+}$ or the catecholate complex $[Cr^{III}(HMC)(TCCat)]^+$, respectively, and an intense spin-forbidden transition ($^4A_2 \rightarrow {}^2E$) was identified for the semiquinonate complexes.[28] Similarly, the reaction between $Cr^{II}(HMC)Cl_2$ and 2,5-dihydroxy-1,4-benzoquinone (H_2DHBQ) afforded a tetraoxolene-bridged Cr^{III} dimer.[20] While these results are interesting, none of the Cr^{III}(HMC) based complexes were structurally characterized, hence leaving the structure−property relationship ambiguous. Additionally, work on Cr(HMC) by Dei focused on species with SQ ligands, leaving species with Cat ligands underexplored.

Described in this contribution are facile preparation of complexes $[1]^+$ ($[Cr(HMC)(catecholate)]^+$), $[2]^+$ ($[Cr(HMC)(tetrachlorocatecholate)]^+$), and $[3]^+$ ($([Cr(HMC)(3,5\text{-di-}tert\text{-butylcatecholate})]^+$, Scheme 2) and subsequent conversion of $[3]^+$ to $[3]^{2+}$ and molecular structures of complexes $[1]^+$, $[2]^+$, $[3]^+$, and $[3]^{2+}$. Complexes $[1]^+$−$[3]^+$ were further characterized with voltammetric and emission spectroscopic techniques. Variable temperature magnetic susceptibility measurements were conducted for complexes $[2]^+$, $[3]^+$, and $[3]^{2+}$. DFT calculations were performed on $[1]^+$, $[2]^+$, $[3]^+$, and $[3]^{2+}$ to better understand the ground-state electronic structures of these complexes.

RESULTS AND DISCUSSION

Synthesis. In general, *cis*-$[Cr(HMC)Cl_2]Cl$ reacted with the corresponding catechol ligand upon *in situ* reduction of Cr^{III} to Cr^{II} using mossy Zn, as shown in Scheme 2. Cr^{III} complexes were formed upon oxidation of Cr^{II} complexes in air. The reaction between *cis*-$[Cr(HMC)Cl_2]Cl$ and 1 equiv of catechol under reflux yielded complex [1]Cl as a forest green powder in 69% yield after purification over a silica plug. Complex [2]Cl was synthesized by using the same procedure and isolated as a sky blue powder in 62% yield after purification. Complex [3]Cl was obtained in a similar manner and isolated as $[3]PF_6$ in 65% yield after an anion exchange using KPF_6(aq) and extraction in EtOAc. Chemical oxidation of $[3]PF_6$ with $FcPF_6$ yields $[3](PF_6)_{1.5}Cl_{0.5}$ (see the discussion below regarding the presence of 0.5 equiv of Cl^-) as a jade green powder in 89% yield. As noted earlier, the previous syntheses of Cr^{III}(HMC) complexes by Dei started from air-sensitive $Cr^{II}(HMC)Cl_2$, and the yields were not reported.[20,28] Our approach, overcoming the kinetic inertness of Cr^{III} through an *in situ* reduction, is more straightforward and could be applicable for preparation of other Cr^{III} complexes.

Molecular Structures. Single crystals of [1]Cl, [2]Cl, $[3]PF_6$, and $[3](PF_6)_{1.5}Cl_{0.5}$ were grown via slow diffusion of hexanes into either a CH_2Cl_2 solution ([1]Cl, [2]Cl) or a benzene solution ($[3]PF_6$) or vapor diffusion of Et_2O into a MeCN solution ($[3](PF_6)_{1.5}Cl_{0.5}$). The molecular structures determined from single crystal X-ray diffraction are shown in Figures 1−4, which show the *cis*-chelation of the catecholate/

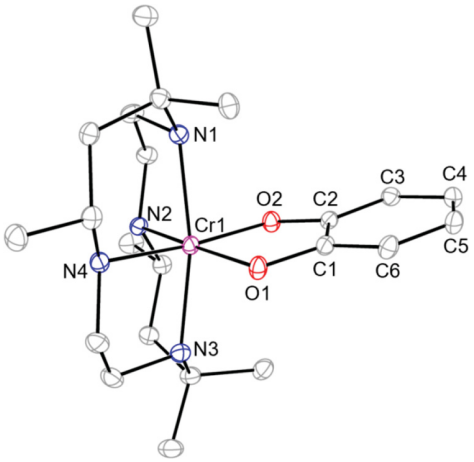

Figure 1. ORTEP plot of $[1]^+$ at the 30% probability level. Hydrogen atoms and Cl^- counteranion are omitted for clarity.

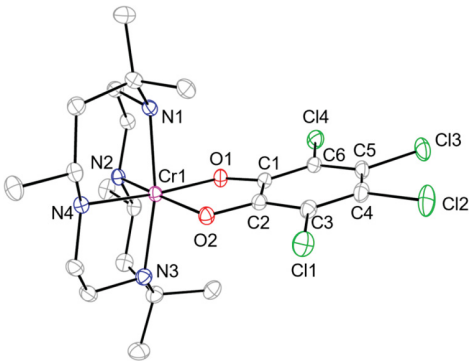

Figure 2. ORTEP plot of $[2]^+$ at the 30% probability level. Hydrogen atoms and Cl^- counteranion are omitted for clarity.

semiquinonate ligand. The N1−Cr1−N3 bond angles, as listed in Table 1, range between 168.48° and 172.68° for all four compounds, indicative of pseudo-octahedral coordination.

The lattice of complex $[3]^{2+}$ contains a cavity in which the hydrogen atoms of N2 and N4 face inward. Strong hydrogen bond interactions paired with the possibility for two cationic units to face each other create an encapsulated point which can contain a single hydrogen bond accepting atom. This results in partial occupation of a Cl^- anion contained in the pocket, which could not be removed despite attempts of anion

https://dx.doi.org/10.1021/acs.inorgchem.0c03224
Inorg. Chem. 2021, 60, 4447−4455

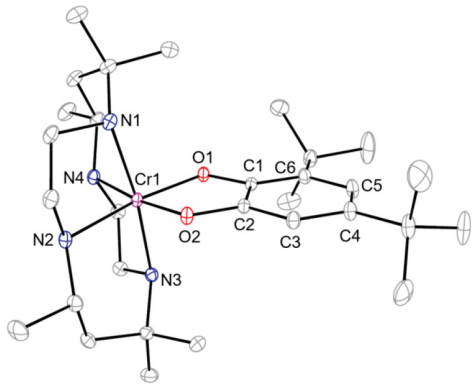

Figure 3. ORTEP plot of $[3]^{+}$ at the 30% probability level. Hydrogen atoms and PF_6^- counteranion are omitted for clarity.

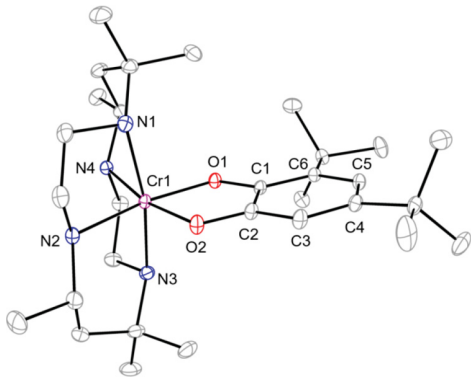

Figure 4. ORTEP plot of $[3]^{2+}$ at the 30% probability level. Hydrogen atoms and counteranions (Cl^- and PF_6^-) are omitted for clarity.

Table 1. Selected Bond Lengths (Å) and Angles (deg) for $[1]^{+}$, $[2]^{+}$, $[3]^{+}$, and $[3]^{2+}$

	$[1]^{+}$	$[2]^{+}$	$[3]^{+}$	$[3]^{2+}$
Cr1−N1	2.143(2)	2.121(2)	2.124(1)	2.140(1)
Cr1−N2	2.112(2)	2.094(1)	2.122(1)	2.094(1)
Cr1−N3	2.138(2)	2.124(2)	2.127(1)	2.135(1)
Cr1−N4	2.122(2)	2.125(1)	2.123(1)	2.089(1)
Cr1−O1	1.940(2)	1.961(1)	1.920(1)	1.9469(9)
Cr1−O2	1.953(1)	1.941(1)	1.908(1)	1.943(1)
O1−C1	1.349(2)	1.341(2)	1.366(2)	1.304(2)
O2−C2	1.365(3)	1.329(2)	1.359(2)	1.301(2)
C1−C2	1.419(3)	1.419(2)	1.411(2)	1.442(2)
C2−C3	1.387(3)	1.387(2)	1.389(2)	1.412(2)
C3−C4	1.396(3)	1.401(2)	1.396(2)	1.370(2)
C4−C5	1.388(3)	1.387(3)	1.400(2)	1.444(2)
C5−C6	1.404(3)	1.405(2)	1.410(2)	1.378(2)
C6−C1	1.387(3)	1.391(2)	1.402(2)	1.428(2)
O1−Cr1−O2	84.56(6)	84.02(5)	85.57(4)	81.27(5)
Cr1−O1−C1	111.31(2)	110.45(5)	111.01(8)	114.93(9)
Cr1−O2−C2	110.52(2)	111.62(5)	111.15(8)	114.4(1)
N1−Cr1−N3	168.64(7)	168.48(6)	172.68(5)	169.06(5)

exchange. The formula is then $[3](PF_6)_{1.5}Cl_{0.5}$ exactly, with one chloride residing on a crystallographic 2-fold axis and being encapsulated between two symmetry-related $[3]^{2+}$. A structural plot depicting two cationic units and the encapsulated chloride anion is provided in Figure S1. A nearly identical formula, "$[Cr(CTH)(DTBSQ)]_2Cl(PF_6)_3$", was proposed based on elemental analysis by Dei.[28] Because the cationic unit of interest is unchanged, and the anion mixture stabilizes the complex, more intensive attempts to remove the Cl^- anion were deemed unnecessary.

It was predicted that $[1]^{+}$−$[3]^{+}$ would be catecholate complexes while the oxidized $[3]^{2+}$ would be a semiquinonate complex. Structural parameters determined are consistent with such designation. The C−C bond lengths within a catechol ring should be nearly identical due to the aromaticity of the ring while the semiquinone species should display alternating bond lengths due to the localization of electrons in double bonds. Upon examining the crystallographic data for $[1]^{+}$, $[2]^{+}$, and $[3]^{+}$, it is evident that they are catecholate complexes. The cyclic C−C bond lengths are similar to one another, and all three complexes exhibit Cr−O bond lengths within the expected range of values for transition metal−catecholate complexes. On the contrary, $[3]^{2+}$ exhibits alternating C−C bond lengths, 1.36−1.45 Å, which is within the documented range for semiquinone species.[29] The intradiol C−O and C1−C2 bond distances can also distinguish between semiquinones (∼1.29 and ∼1.44 Å, respectively) and catecholates (∼1.35 and 1.39 Å, respectively), further supporting the assignment of $[1]^{+}$−$[3]^{+}$ as catecholates and $[3]^{2+}$ as a semiquinonate.[30] Further supporting the delocalization of the SQ charge, the Cr−O1 and Cr−O2 bond lengths in $[3]^{2+}$ are identical with the experimental errors, and these bonds are slightly elongated from those in $[3]^{+}$. Sato and co-workers observed comparable Cr−O bond distances in the crystal structure of $[(Cr(CTH))(Co(CTH))(\mu\text{-dhbq})](PF_6)_3$ at 200 K (1.933 and 1.940 Å), where Cr^{III} is coordinated to a bridging semiquinonate ligand.[31] To compensate for the reduced donicity of SQ compared to CAT in $[3]^{2+}$, the nitrogen centers trans to SQ (N2 and N4) are about 0.045 Å closer to the Cr center than the other two nitrogens (N1 and N3).

Electrochemistry. Electrochemical measurements in MeCN indicate that all three complexes undergo a reversible one-electron oxidation. The anodic cyclic voltammograms are presented in Figure 5 while the redox potentials are given in Table 2. These redox events are ligand-centered, resulting from the conversion of catecholate to semiquinonate. The

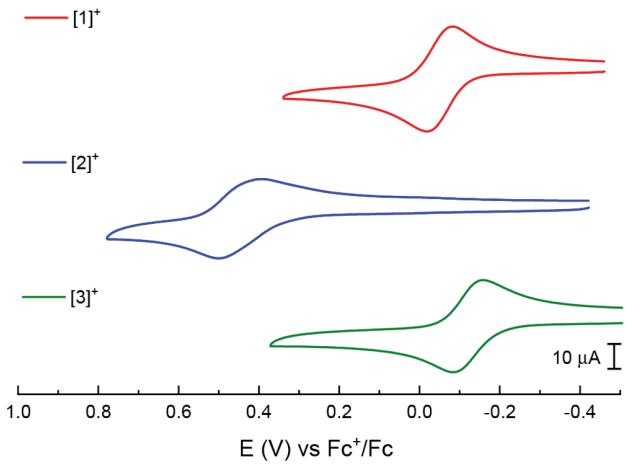

Figure 5. Cyclic voltammograms of $[1]^{+}$ (top), $[2]^{+}$ (middle), and $[3]^{+}$ (bottom) recorded at a 0.1 V/s scan rate in a 1.0 mM MeCN solution of 0.2 M n-Bu_4NPF_6.

https://dx.doi.org/10.1021/acs.inorgchem.0c03224
Inorg. Chem. 2021, 60, 4447−4455

Table 2. Electrochemical Potentials (V, vs Fc^+/Fc) for $[1]^+$–$[3]^+$

	E(Cat/SQ)	E(SQ/BQ)[a]
$[1]^+$	−0.043	1.40
$[2]^+$	0.415	1.58
$[3]^+$	−0.114	1.03

[a]Irreversible couple; E_{pa} is reported.

oxidations for [Cr(CTH)TCCat]PF_6 and [Cr(CTH)TBCat]Cl were previously reported at 0.84 and 0.21 V (vs SCE),[28] which are close to our reported values. Irreversible oxidations for the conversion of semiquinonate to quinonate were observed at 1.40 V (vs Fc^+/Fc) for $[1]^+$, 1.58 V for $[2]^+$, and 1.03 V for $[3]^+$ (Figure S2). No chromium-based redox events occurred within the solvent window. The di-*tert*-butyl substituents have a marginal effect on the redox properties of the catecholate, shifting the redox potential of $[3]^+$ cathodically by 0.071 V with respect to that of $[1]^+$. On the contrary, the tetrachloro substitution has a profound effect, shifting the potential of $[2]^+$by 0.46 V anodically from that of $[1]^+$.

UV–Vis Spectroscopic Analysis. The UV–vis absorption spectra of $[1]^+$, $[2]^+$, and $[3]^+$ recorded in MeCN are shown in Figure 6. Spin-allowed d–d transitions occur between 500 and

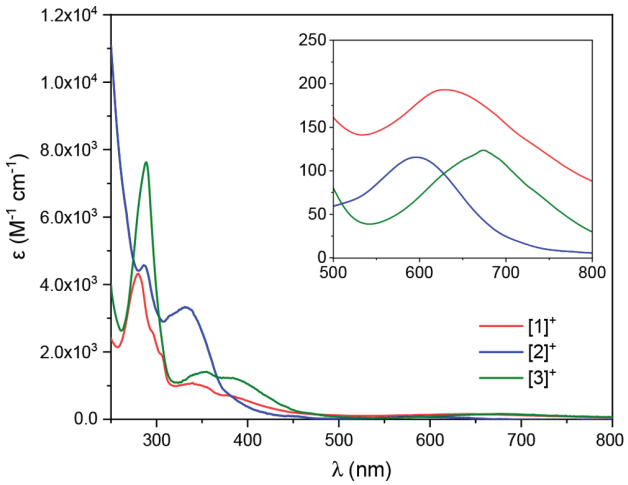

Figure 6. Absorption spectra of $[1]^+$, $[2]^+$, and $[3]^+$ in MeCN with d–d transitions magnified in the inset.

800 nm, as highlighted in the inset. Compared to $[1]^+$ (λ_{max} at 629 nm), the λ_{max} of $[2]^+$ is blue-shifted to 596 nm, while that of $[3]^+$ is red-shifted to 678 nm. Because intraligand ($n \rightarrow \pi^*$ and $\pi \rightarrow \pi^*$) transitions or charge-transfer (MLCT or LMCT) transitions are possible in the UV region, a solvent dependence study was conducted in MeOH, THF, and EtOAc in addition to MeCN (Figure S3). While the molar absorptivity varied depending on the solvent, the λ_{max} values for the two transitions were nearly identical, ranging between 351–354 nm and 377–380 nm (Table S2). This indicates that they are most likely intraligand in nature, although it should be noted that not all charge-transfer bands are solvatochromic.[32]

The absorption spectra of $[3]^+$ and $[3]^{2+}$ recorded in MeCN are shown in Figure 7, while the spectral series of $[3]^+$ being oxidized to $[3]^{2+}$ while holding the potential at 0.43 V is provided in Figure S4. Spectral assignments for $[3]^{2+}$ were previously suggested by Dei and Benelli.[28] A prominent feature

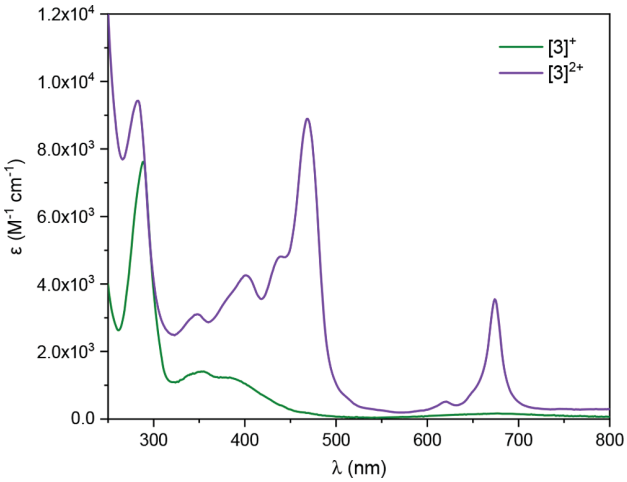

Figure 7. Absorption spectrum of $[3]^+$ and $[3]^{2+}$ in MeCN.

is the intense, sharp transition observed at 674 nm, which is attributed to a spin-forbidden transition of $^4A_2(Cr^{III}) \rightarrow {}^2E(SQ)$ parentage with an effective C_{2v} symmetry. This is due to strong exchange coupling between Cr^{III} and the SQ radical. Intense transitions observed at 469 and 440 nm have been previously assigned as MLCT in nature because of the observed red-shift in the presence of electron-withdrawing groups on the semiquinone ligand.[28] Intraligand transitions appear below 400 nm.

Emission Studies. The emission spectra of $[1]^+$–$[3]^+$ in 2-methyltetrahydrofuran glass at 77 K are shown in Figure 8, with phosphorescence lifetimes reported in Table 3. Because of low symmetry, the emissive state for Cr^{III} can sometimes be difficult to assign, and thus the lowest-energy state may not be of ^2E parentage. For example, Forster has documented that the energy of the $^2T_1$ state can drop below that of the ^2E state in the presence of a strongly tetragonal ligand field, as in the cases of *trans*-$[Cr(cyclam)F_2]^+$ and *trans*-$[Cr(HMC)F_2]^+$.[17] The ^2E emission spectra are typically narrow, while those of $^2T_1$ are broad. Nevertheless, spectral shape alone is insufficient to make a formal assignment.

All three catecholate complexes exhibit ^2E emission with a λ_{max} ranging between 720 and 730 nm. Although ^2E emission for Cr^{III} complexes typically occurs between 660 and 700 nm, it has been documented that the emission red-shifts upon increasing the number of N–H bonds directly bound to the metal center.[33] McCusker and co-workers reported ^2E emission of [Cr(tren)(DTBCat)]PF_6 (tren = tris(2-aminoethyl)amine) centered at 725 nm with a lifetime of 50 μs,[34] which is comparable to $[1]^+$ with a lifetime of 50 μs and $[3]^+$ with a lifetime of 57 μs. Other *cis*-$[Cr^{III}N_4X_2]^+$ type complexes have displayed similar phosphorescence lifetimes.[33]

The spectrum of $[2]^+$ is quite different from those of $[1]^+$ and $[3]^+$. While $[2]^+$ exhibits ^2E emission around the same wavelength as $[1]^+$ and $[3]^+$, an intense, but shorter lived emission from the $^2T_1$ state is also observed centered at 762 nm. Although the energy levels of doublet states, such as $^2T_1$, are not influenced by ligand field strength, they are impacted by the nephelauxetic effect.[17] The delocalization of electrons over the catecholate ligand and away from the Cr^{III} center reduces repulsion and expands the electron cloud, resulting in lower energy emission. Revisiting the crystallographic data of $[1]^+$–$[3]^+$, it is evident that $[2]^+$ possesses the longest Cr–O

https://dx.doi.org/10.1021/acs.inorgchem.0c03224
Inorg. Chem. 2021, 60, 4447–4455

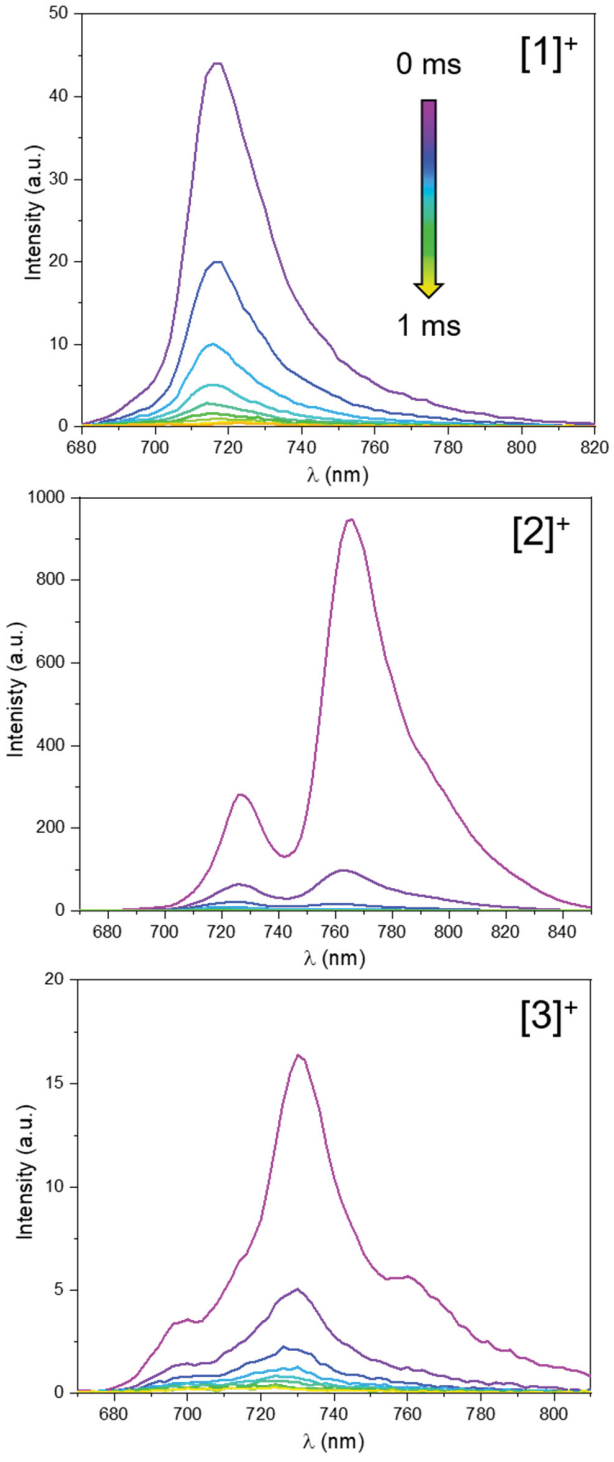

Figure 8. Time-delayed emission spectra of $[1]^+$ (top), $[2]^+$ (middle), and $[3]^+$ (bottom) at 77 K in 2-methyltetrahydrofuran at varying delay times.

bond lengths of the series. The $^2T_1$ energy is lowered below the ^2E state, and dual emission is observed.

Phosphorescence was not observed for $[3]^{2+}$ at 77 K in 2-methyltetrahydrofuran between 600 and 800 nm, which is consistent with the absence of emission in [Cr(tren)3,6-DTBSQ]$(PF_6)_2$ reported by McCusker.[34] If emission is present, it may be short-lived and not measurable on the time scale of our instrument.

Table 3. Photophysical Data for Complexes $[1]^+$, $[2]^+$, and $[3]^+$

	$\tau(^2E)$ (μs)	$\tau(^2T_1)$ (μs)	λ_{ex} (nm)	λ_{max} (nm)
$[1]^+$	50		340	720
$[2]^+$	38	22	350	726, 762
$[3]^+$	57		340	730

Temperature-Dependent Magnetic Susceptibility. Magnetic susceptibility measurements can provide insight into the differences between electron-donating and -withdrawing groups on catecholate, in addition to the contrast in ground-state configurations between catecholate and semiquinone complexes. Effective magnetic moments for solid state samples of complexes $[2]^+$, $[3]^+$, and $[3]^{2+}$ between 1.8 and 300 K are shown in Figure 9. The observed magnetic moment

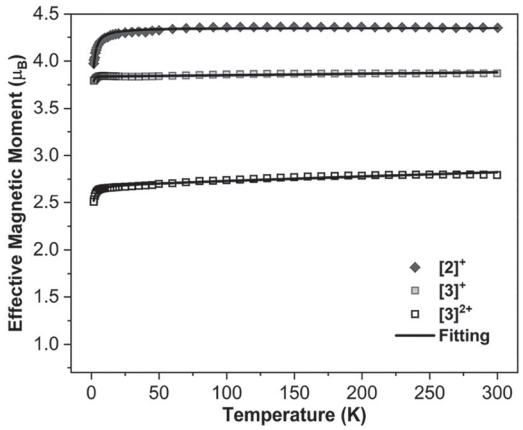

Figure 9. Temperature-dependent magnetic susceptibility of catecholate complexes $[2]^+$ and $[3]^+$ as well as semiquinonate complex $[3]^{2+}$ from 1.8 to 300 K. The solid lines represent the fitting results.

for $[3]^+$ at 300 K is 3.88 μ_B, which is in excellent agreement with the expected value of 3.87 μ_B for a spin-only Cr^{III} ion (S = 3/2). However, $[2]^+$ has an effective magnetic moment of 4.35 μ_B at 300 K, which is higher than expected. This could be due to a larger Landé factor caused by the spin−orbital coupling of Cr^{III} ion. The effective magnetic moment of $[3]^{2+}$ is expected to have a spin-only value of 2.83 μ_B, resulting from the very strong antiferromagnetic coupling of Cr^{III} (S = 3/2) and the semiquinone ligand (S = 1/2) to yield an S = 1 system. It is worth mentioning that instead of superexchange, the coupling in $[3]^{2+}$ is direct exchange in nature due to the proximity of SQ and Cr(III), which is similar to the case of N_2^{3-} radical-bridged terbium complex.[35] The observed magnetic moment of $[3]^+$ at 300 K is 2.79 μ_B, which is in good agreement with the spin-only value. Dei reported an effective magnetic moment of 2.9 μ_B at room temperature for [Cr(CTH)(3,5-DTBSQ)]$_2(PF_6)_3Cl$, which is similar to our reported value. While the effective magnetic moments remain nearly constant between 25 and 300 K for all three complexes, small decreases are observed below 25 K, which are mainly ascribed to the zero-field splitting effect (see the Supporting Information for details). Plots of $\chi_M T$ vs T and M vs H can be found in Figures S5 and S6.

https://dx.doi.org/10.1021/acs.inorgchem.0c03224
Inorg. Chem. 2021, 60, 4447−4455

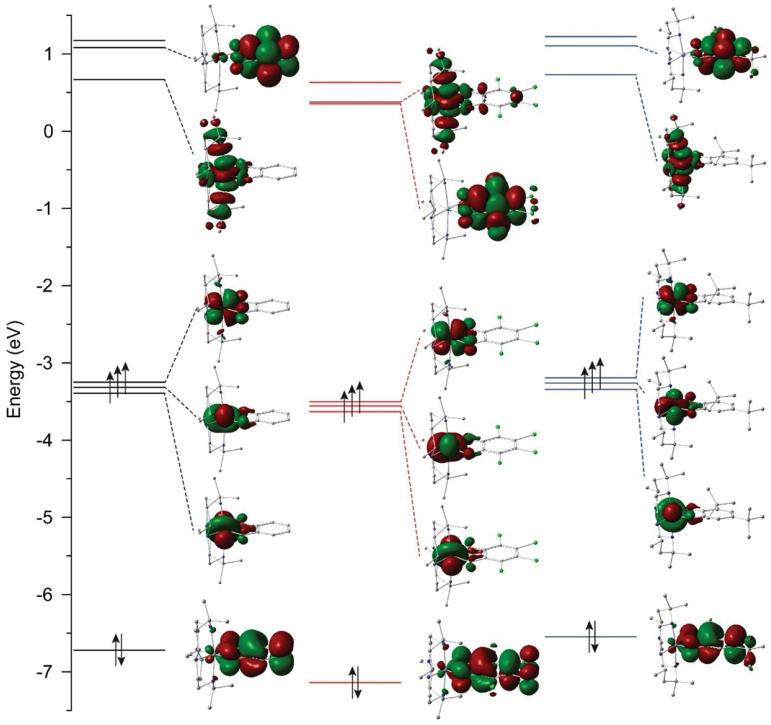

Figure 10. Frontier molecular orbitals of $[\mathbf{1}]^+$ (left), $[\mathbf{2}]^+$ (center), and $[\mathbf{3}]^+$ (right) derived from DFT calculations. MOs are plotted at lisovaluel = 0.025.

Density Functional Theory (DFT) Calculations. To better understand the ground-state electronic structures of Cr^{III}(HMC) catecholate complexes, DFT calculations were performed on the monocationic complexes $[\mathbf{1}]^+$–$[\mathbf{3}]^+$; frontier molecular orbitals (MOs) for all three are shown in Figure 10. In the quartet ground state, which has been verified by using magnetic susceptibility measurements, the three singly occupied MOs (SOMO, SOMO−1, and SOMO−2) belong to the near-degenerate set of d_{xy}, d_{yz}, and d_{xz} orbitals. The highest fully occupied orbital is almost exclusively catecholate-based, with negligible contributions from Cr and the HMC ligand. The difference between $[\mathbf{2}]^+$ and the other two complexes lies in the ordering of the lowest unoccupied orbitals LUMO−LUMO+2. In the cases of $[\mathbf{1}]^+$ and $[\mathbf{3}]^+$, the LUMO is a d_{z^2} orbital, which is ca. 0.4 eV lower than the predominantly catecholate-based LUMO+1. Reflecting the strong electron-withdrawing nature of four chloro substituents, the LUMO of $[\mathbf{2}]^+$ is entirely catecholate-based, with a very closely spaced (ca. 0.02 eV) LUMO+1 of d_{z^2} character. In all three complexes, the presence of both the catecholate oxygens and the HMC nitrogens in the equatorial plane raises the energy of the $d_{x^2-y^2}$ over the d_{z^2} orbital to the LUMO+2 (not pictured). Considering that the occupied orbitals do not substantially differ among the three complexes, it is likely that the differences seen in the emission spectra of $[\mathbf{1}]^+/[\mathbf{3}]^+$ and $[\mathbf{2}]^+$ (Figure 8) arise due to the differences in relative ordering of the unoccupied orbitals.

Furthermore, ground-state DFT calculations performed on the oxidized, dicationic complex $[\mathbf{3}]^{2+}$ corroborate the antiferromagnetic coupling between the S = 3/2 Cr^{III} and S = 1/2 semiquinone ligand. Spin-density calculations place three unpaired electrons on Cr and one unpaired electron mainly delocalized over the O1, C1, C2, and O2 atoms (Figure S8). In accordance with the radical anionic nature of the ligand, the experimentally observed alternating C−C/C═C bond lengths of the semiquinone ligand are faithfully reproduced by DFT (Table S3).

CONCLUSION

Three Cr^{III}(HMC) complexes bearing catecholate ligands and one complex bearing a semiquinonate ligand were prepared and characterized. Bond lengths confirmed the oxidation state of the Cat/SQ ligands. Among the catecholate series, it is evident that the electron-donating groups in $[\mathbf{3}]^+$ result in properties similar to $[\mathbf{1}]^+$, while electron-withdrawing groups in $[\mathbf{2}]^+$ result in significantly larger deviations from $[\mathbf{1}]^+$. The most noteworthy differences with $[\mathbf{2}]^+$ are that the reversible Cat/SQ oxidation is shifted by 0.458 V compared to $[\mathbf{1}]^+$, and there is dual emission from the ^2E and $^2T_1$ states (instead of solely ^2E emission). Comparison of $[\mathbf{3}]^+$ and $[\mathbf{3}]^{2+}$ showed that the semiquinonate ligand displayed rich absorption spectra with a spin-forbidden transition. The magnetic susceptibility indicated there is strong antiferromagnetic coupling between the Cr(III) (S = 3/2) and SQ (S = 1/2) ligand in $[\mathbf{3}]^{2+}$, resulting in an effective magnetic moment of 2.83 μ_B at 300 K, which closely aligns with the spin-only value expected for an S = 1 system.

EXPERIMENTAL SECTION

Materials. Catechol was purchased from Alfa Aesar, 3,5-di-*tert*-butylcatechol from ACROS Organics, mossy zinc from Mallinckrodt Chemical Works, and methanol from Fisher. HMC,[36] *cis*-[Cr(HMC)-Cl_2]Cl,[37] and 3,4,5,6-tetrachlorocatechol[38] were prepared by using literature procedures. All reactions were performed in an open atmosphere.

Physical Measurements. UV−vis spectra were obtained with a JASCO V-670 spectrophotometer. ESI-MS were analyzed on an Advion mass spectrometer. Emission studies were performed on a

https://dx.doi.org/10.1021/acs.inorgchem.0c03224
Inorg. Chem. 2021, 60, 4447−4455

Varian Cary Eclipse fluorescence spectrophotometer. Cyclic voltammograms were recorded in 0.2 M n-Bu_4NPF_6 solution (MeCN, N_2-degassed) on a CHI620A voltammetric analyzer with a glassy carbon working electrode, a Pt-wire auxiliary electrode, and an Ag/AgCl reference electrode with ferrocene used as an external reference. Spectrochemical analysis was performed by using an OTTLE (optically transparent thin-layer electrochemical) liquid-sample cell with a 0.2 mm optical path length, 0.3 mL sample volume, and a CaF_2 window procured from F. Hartl, Reading, UK. The cell was equipped with a mesh Pt working electrode, a mesh Pt auxiliary electrode, and an Ag reference electrode. The analyte concentration was 1.0 mM in 4 mL of dry MeCN at a 0.1 M n-Bu_4NPF_6 electrolyte concentration. The temperature-dependent magnetic susceptibility was measured on a MPMS-XL7 SQUID magnetometer. Elemental analysis was performed by Atlantic Microlab, Inc. (Norcross, GA).

*Synthesis of cis-[Cr(HMC)(catecholate)]Cl ([**1**]Cl).* *cis*-[Cr(HMC)-Cl_2]Cl (0.241 g, 0.545 mmol) and catechol (0.120 g, 1.09 mmol) were combined in 30 mL of methanol with ∼0.5 g of mossy zinc. The reaction mixture was stirred and refluxed for 6 h. The crude reaction mixture was purified over a silica gel plug by using CH_2Cl_2, 1:1 CH_2Cl_2:MeCN, MeCN, 2:1 MeCN:MeOH, and MeOH. The product was recrystallized from CH_2Cl_2/Et_2O to give [**1**]Cl as a dark green solid (69% based on Cr). ESI-MS [M^+] 444 m/z, where [M^+] denotes the cationic species of [**1**]$^+$. Elem. Anal. Found (Calcd) for *cis*-[Cr(HMC)(catecholate)]Cl·1CH_2Cl_2: C, 48.60 (48.90); H, 7.66 (7.49); N, 9.53 (9.92). CV [$E_{1/2}$/V, ΔE_p/V, $i_{backward}/i_{forward}$]: Cat/SQ, −0.43, 0.063, 0.94; E_{pa} SQ/BQ, 1.40. UV−vis, λ_{max}/nm (ε/M^{-1} cm^{-1}): 629 (193), 370 (733), 340 (1080), 312 (sh), 293 (sh), 280 (4320).

*Synthesis of cis-[Cr(HMC)(3,4,5,6-tetrachlorocatecholate)]Cl ([**2**]Cl).* *cis*-[Cr(HMC)Cl_2]Cl (0.100 g, 0.226 mmol) and 3,4,5,6-tetrachlorocatechol (0.056 g, 0.226 mmol) were combined in 30 mL of methanol with ∼0.5 g of mossy zinc. The reaction mixture was stirred and refluxed for 3 h. The crude reaction mixture was purified over a silica gel plug, and [**2**]Cl was eluted with 2:1 MeCN:MeOH. The product was a sky blue solid (62% based on Cr). Product was recrystallized with DCM/Et_2O. ESI-MS [M^+] 582 m/z, where [M^+] denotes the cationic species of [**2**]$^+$. Elem. Anal. Found (Calcd) for *cis*-[Cr(HMC)(3,4,5,6-tetrachlorocatecholate)]Cl·1.5CH_2Cl_2: C, 37.36 (37.88); H, 5.18 (5.27); N, 7.71 (7.52). CV [$E_{1/2}$/V, ΔE_p/V, $i_{backward}/i_{forward}$]: Cat/SQ, −0.415, 0.105, 0.93; E_{pa} SQ/BQ, 1.58. UV−vis, λ_{max}/nm (ε/M^{-1} cm^{-1}): 596 (117), 333 (3320), 286 (4570).

*Synthesis of [Cr(HMC)(3,5-di-tert-butylcatecholate)](PF$_6$) ([**3**]PF$_6$).* *cis*-[Cr(HMC)Cl_2]Cl (0.500 g, 0.113 mmol) and 3,5-di*tert*-butylcatechol (0.025 g, 0.114 mmol) were combined in 30 mL of methanol with ∼0.5 g of mossy zinc. The reaction mixture was stirred and refluxed for 18 h. The crude reaction mixture was filtered, and solvent volume was reduced by using a rotary evaporator. A saturated aqueous solution of KPF_6 was added to the crude reaction mixture. The product was extracted with EtOAc. The solvent was removed, and the product was dissolved in THF. The product [**3**]PF_6 was obtained by adding hexanes to THF to yield a lime green solid (65% based on Cr). ESI-MS [M^+] 557 m/z, where [M^+] denotes the cationic species of [**3**]$^+$. Elem. Anal. Found (Calcd) for *cis*-[Cr(HMC)(3,5-di-*tert*-butylcatecholate)](PF_6): C, 50.93 (51.35); H, 8.13 (8.04); N 7.59 (7.98). CV [$E_{1/2}$/V, ΔE_p/V, $i_{backward}/i_{forward}$]: Cat/SQ, −0.114, 0.075, 0.95; E_{pa} SQ/BQ, 1.03. UV−vis, λ_{max}/nm (ε/M^{-1} cm^{-1}): 678 (167), 351 (1690), 372 (1430), 289 (8150).

*Synthesis of [Cr(HMC)3,5-di-tert-butylsemiquinonate](PF$_6$)$_{1.5}$Cl$_{0.5}$ ([**3**](PF$_6$)$_{1.5}$Cl$_{0.5}$).* Ferrocenium hexafluorophosphate (23.5 mg, 0.0711 mmol) was added to a solution of [**3**]PF_6 (0.050 g, 0.0711 mmol) in MeCN and was stirred for 30 min. The remaining $FcPF_6$ was filtered off. A jade green solid was precipitated out by adding hexanes to a solution of [**3**]$^{2+}$ in THF or CH_2Cl_2. The solid was washed with hexanes to remove any remaining ferrocene. The product was recrystallized with MeCN/Et_2O to result in a jade green solid (89% based on [**3**]PF_6). Elem. Anal. Found (Calcd) for *cis*-[Cr(HMC)(3,5-ditertbutylsemiquinone)](PF_6)$_{1.5}$$Cl_{0.5}$·2$CH_2Cl_2$: C, 40.26 (39.96); H, 6.43 (6.29); N, 5.88 (5.82). UV−vis, λ_{max}/nm (ε/M^{-1} cm^{-1}): 674 (3548), 652 (sh), 621 (515), 469 (8895), 440 (4810), 400 (4260), 348 (3100), 283 (9433).

X-ray Crystallographic Analysis. X-ray diffraction data for [**1**]Cl, [**2**]Cl, [**3**]PF_6, and [**3**](PF_6)$_{1.5}$$Cl_{0.5}$ were collected at 150 K on a Bruker Quest diffractometer with Mo Kα radiation (λ = 0.71073 Å). Data were collected and processed by using APEX3 and reduced by using SAINT.[39] The structures were solved by using the SHELXTL suite of programs and refined by using Shelxl2016.[40] Details of data collection and structure refinement are provided in Table S1.

Computational Details. All DFT calculations were performed by using Gaussian 16, Rev. A.03.[41] Geometry optimizations were performed on [**1**]$^+$, [**2**]$^+$, [**3**]$^+$, and [**3**]$^{2+}$ by using their respective X-ray structures as initial geometries. Minima were confirmed by using frequency analyses; no imaginary frequencies were found. Calculations were attempted by using multiple functionals. Data from emission spectra (phosphorescence) were used as a constraint for the minimum-energy difference between the quartet ground state and the doublet excited state. Based on this, the M06-2X functional[42] was found to perform satisfactorily for both complexes. The def2tzvp basis set was used for Cr and the def2svp basis set for all other atoms.[43] Dispersion forces were modeled by using Grimme's D3 empirical dispersion model.[44] All calculations were performed in acetonitrile as solvent described by using the polarizable continuum model (PCM).[45]

■ ASSOCIATED CONTENT

Supporting Information

The Supporting Information is available free of charge at https://pubs.acs.org/doi/10.1021/acs.inorgchem.0c03224.

Crystallographic information for all complexes, hydrogen-bonding illustration between Cl^- and two [**3**]$^{2+}$ cations, cyclic voltammetry, solvatochromatic study of [**3**]$^+$, spectroelectrochemical characterization of [**3**]$^{1+/2+}$, temperature-dependent magnetic measurements of complexes [**2**]$^+$, [**3**]$^+$, and [**3**]$^{2+}$, and further DFT characterization (PDF)

Accession Codes

CCDC 2039087−2039090 contain the supplementary crystallographic data for this paper. These data can be obtained free of charge via www.ccdc.cam.ac.uk/data_request/cif, or by emailing data_request@ccdc.cam.ac.uk, or by contacting The Cambridge Crystallographic Data Centre, 12 Union Road, Cambridge CB2 1EZ, UK; fax: +44 1223 336033.

■ AUTHOR INFORMATION

Corresponding Author

Tong Ren − *Department of Chemistry, Purdue University, West Lafayette, Indiana 47907, United States;* orcid.org/0000-0002-1148-0746; Email: tren@purdue.edu

Authors

Ashley J. Schuman − *Department of Chemistry, Purdue University, West Lafayette, Indiana 47907, United States*

Adharsh Raghavan − *Department of Chemistry, Purdue University, West Lafayette, Indiana 47907, United States*

Susannah D. Banziger − *Department of Chemistry, Purdue University, West Lafayette, Indiana 47907, United States*

You Song − *State Key Laboratory of Coordination Chemistry, School of Chemistry and Chemical Engineering, Nanjing University, Nanjing 210023, China;* orcid.org/0000-0002-0289-7830

Zhao-Bo Hu − *State Key Laboratory of Coordination Chemistry, School of Chemistry and Chemical Engineering, Nanjing University, Nanjing 210023, China;* orcid.org/0000-0001-9266-6624

https://dx.doi.org/10.1021/acs.inorgchem.0c03224
Inorg. Chem. 2021, 60, 4447−4455

Brandon L. Mash − *Department of Chemistry, Purdue University, West Lafayette, Indiana 47907, United States*
Andrew L. Williams − *Department of Chemistry, Purdue University, West Lafayette, Indiana 47907, United States*

Complete contact information is available at: https://pubs.acs.org/10.1021/acs.inorgchem.0c03224

Notes

The authors declare no competing financial interest.

■ ACKNOWLEDGMENTS

We thank both the National Science Foundation (CHE 1764347 and CHE 1625543 at Purdue) and the National Natural Science Foundation of China (No. 21973038 at Nanjing) for generously supporting this work.

■ REFERENCES

(1) Broere, D. L. J.; Plessius, R.; van der Vlugt, J. I. New avenues for ligand-mediated processes - expanding metal reactivity by the use of redox-active catechol, o-aminophenol and o-phenylenediamine ligands. *Chem. Soc. Rev.* **2015**, *44*, 6886−6915.
(2) Chirik, P. J.; Wieghardt, K. Radical Ligands Confer Nobility on Base Metal Catalysts. *Science* **2010**, *327*, 794−795.
(3) Pierpont, C. G.; Lange, C. W. The Chemistry of Transition Metal Complexes Containing Catechol and Semiquinone Ligands. *Prog. Inorg. Chem.* **1994**, *41*, 331−442.
(4) Kaim, W. Manifestations of Noninnocent Ligand Behavior. *Inorg. Chem.* **2011**, *50*, 9752−9765.
(5) Pierpont, C. G.; Kelly, J. K. *PATAI'S Chemistry of Functional Groups*, 2014.
(6) Kaim, W.; Schwederski, B. Non-innocent ligands in bioinorganic chemistry - An overview. *Coord. Chem. Rev.* **2010**, *254*, 1580−1588.
(7) Kumar, P.; Lindeman, S. V.; Fiedler, A. T. Cobalt Superoxo and Alkylperoxo Complexes Derived from Reaction of Ring-Cleaving Dioxygenase Models with O-2. *J. Am. Chem. Soc.* **2019**, *141*, 10984−10987.
(8) Sahu, S.; Goldberg, D. P. Activation of Dioxygen by Iron and Manganese Complexes: A Heme and Nonheme Perspective. *J. Am. Chem. Soc.* **2016**, *138*, 11410−11428.
(9) Bittner, M. M.; Lindeman, S. V.; Fiedler, A. T. A Synthetic Model of the Putative Fe(II)-Iminobenzosemiquinonate Intermediate in the Catalytic Cycle of o-Aminophenol Dioxygenases. *J. Am. Chem. Soc.* **2012**, *134*, 5460−5463.
(10) Gütlich, P.; Dei, A. Valence Tautomeric Interconversion in Transition Metal 1,2-Benzoquinone Complexes. *Angew. Chem., Int. Ed. Engl.* **1997**, *36*, 2734−2736.
(11) Tezgerevska, T.; Alley, K. G.; Boskovic, C. Valence tautomerism in metal complexes: Stimulated and reversible intramolecular electron transfer between metal centers and organic ligands. *Coord. Chem. Rev.* **2014**, *268*, 23−40.
(12) Kitagawa, S.; Kawata, S. Coordination compounds of 1,4-dihydroxybenzoquinone and its homologues. Structures and properties. *Coord. Chem. Rev.* **2002**, *224*, 11−34.
(13) Demir, S.; Jeon, I. R.; Long, J. R.; Harris, T. D. Radical ligand-containing single-molecule magnets. *Coord. Chem. Rev.* **2015**, *289*, 149−176.
(14) DeGayner, J. A.; Jeon, I. R.; Sun, L.; Dinca, M.; Harris, T. D. 2D Conductive Iron-Quinoid Magnets Ordering up to T-c = 105 K via Heterogenous Redox Chemistry. *J. Am. Chem. Soc.* **2017**, *139*, 4175−4184.
(15) Liu, L. J.; Li, L.; DeGayner, J. A.; Winegar, P. H.; Fang, Y.; Harris, T. D. Harnessing Structural Dynamics in a 2D Manganese-Benzoquinoid Framework To Dramatically Accelerate Metal Transport in Diffusion-Limited Metal Exchange Reactions. *J. Am. Chem. Soc.* **2018**, *140*, 11444−11453.
(16) Kirk, A. D. Photochemistry and Photophysics of Chromium-(III) Complexes. *Chem. Rev.* **1999**, *99*, 1607−1640.
(17) Forster, L. S. The photophysics of chromium(III) complexes. *Chem. Rev.* **1990**, *90*, 331−353.
(18) Kane-Maguire, N. A. P. In *Photochemistry and Photophysics of Coordination Compounds I*; Balzani, V., Campagna, S., Eds., 2007; Vol. *280*, pp 37−67.
(19) Pei, Y.; Journaux, Y.; Kahn, O.; Dei, A.; Gatteschi, D. A Mn-II-Cu-II-Mn-II Trinuclear Species with an S = 9/2 Ground-State. *J. Chem. Soc., Chem. Commun.* **1986**, 1300−1301.
(20) Dei, A.; Gatteschi, D.; Pardi, L.; Russo, U. Tetraoxolene Radical Stabilization by the Interaction with Transition-Metal Ions. *Inorg. Chem.* **1991**, *30*, 2589−2594.
(21) Dei, A.; Gatteschi, D.; Pardi, L. Synthesis, Characterization, and Reactivity of Catecholato Adducts of Iron(III) Triazaazamacrocyclic and Tetraazamacrocyclic Complexes - Chemical Evidence of the Role of the Metal-Ion in the Oxidative Cleavage. *Inorg. Chem.* **1993**, *32*, 1389−1395.
(22) Benelli, C.; Dei, A.; Gatteschi, D.; Pardi, L. Redox Potentials and Charge-Transfer Spectra of Catecholate and Semiquinone Adducts of a Cobalt Tetraazamacrocyclic Complex. *Inorg. Chim. Acta* **1989**, *163*, 99−104.
(23) Caneschi, A.; Dei, A.; Fabrizi de Biani, F.; Gutlich, P.; Ksenofontov, V.; Levchenko, G.; Hoefer, A.; Renz, F. Pressure- and temperature-induced valence tautomeric interconversion in a o-dioxolene adduct of a cobalt-tetraazamacrocycle complex. *Chem. - Eur. J.* **2001**, *7*, 3926−3930.
(24) Benelli, C.; Dei, A.; Gatteschi, D.; Pardi, L. Synthesis, Redox Behavior, Magnetic-Properties, and Crystal-Structure of a Nickel(II)-Semiquinone Adduct with an Unusually Strong Ferromagnetic Coupling. *Inorg. Chem.* **1988**, *27*, 2831−2836.
(25) Dei, A.; Pardi, L. Electronic-Structure of Dioxolene Adducts of Rhodium(III) Tetraazamacrocyclic Complexes. *Inorg. Chim. Acta* **1991**, *181*, 3−5.
(26) Dei, A.; Gatteschi, D.; Pardi, L. Sextet Ground-State in a Dinuclear Nickel(II) Complex Containing a Tetraoxolene Radical as Bridging Ligand. *Inorg. Chim. Acta* **1991**, *189*, 125−128.
(27) Bencini, A.; Carbonera, C.; Dei, A.; Vaz, M. G. F. Magnetic exchange interaction between paramagnetic transition metal ions and radical ligands. A 9,10-dioxophenanthrenesemiquinonato adduct of a nickel(II)-tetraazamacrocycle complex and DFT description. *Dalton Trans.* **2003**, 1701−1706.
(28) Benelli, C.; Dei, A.; Gatteschi, D.; Gudel, H. U.; Pardi, L. Large Intensity Enhancement of the Spin-Forbidden 4a2g- 2eg Transition in Chromium(III) Semiquinone Complexes. *Inorg. Chem.* **1989**, *28*, 3089−3091.
(29) Brown, S. N. Metrical Oxidation States of 2-Amidophenoxide and Catecholate Ligands: Structural Signatures of Metal Ligand Bonding in Potentially Noninnocent Ligands. *Inorg. Chem.* **2012**, *51*, 1251−1260.
(30) Zanello, P.; Corsini, M. Homoleptic, mononuclear transition metal complexes of 1,2-dioxolenes: Updating their electrochemical-to-structural (X-ray) properties. *Coord. Chem. Rev.* **2006**, *250*, 2000−2022.
(31) Kanegawa, S.; Shiota, Y.; Kang, S.; Takahashi, K.; Okajima, H.; Sakamoto, A.; Iwata, T.; Kandori, H.; Yoshizawa, K.; Sato, O. Valence tautomerism in metal complexes: Stimulated and reversible intramolecular electron transfer between metal centers and organic ligands. *J. Am. Chem. Soc.* **2016**, *138*, 14170−14173.
(32) Lever, A. B. P. *Inorganic Electronic Spectroscopy*, 2nd ed.; Elsevier: New York, 1984.
(33) Forster, L. S.; Moensted, O. Low temperature luminescence of chromium(III) complexes coordinated with macrocyclic tetraamine ligands. *J. Phys. Chem.* **1986**, *90*, 5131−5134.
(34) Wheeler, D. E.; McCusker, J. K. Electron Exchange and the Photophysics of Metal-Quinone Complexes. 1. Synthesis and Spectroscopy of Chromium-Quinone Dyads. *Inorg. Chem.* **1998**, *37*, 2296−2307.
(35) Rinehart, J. D.; Fang, M.; Evans, W. J.; Long, J. R. A N-2(3-) Radical-Bridged Terbium Complex Exhibiting Magnetic Hysteresis at 14 K. *J. Am. Chem. Soc.* **2011**, *133*, 14236−14239.

(36) Hay, R. W.; Lawrance, G. A.; Curtis, N. F. A convenient synthesis of the tetra-aza-macrocyclic ligands trans-[14]-diene, tet a, and tet b. *J. Chem. Soc., Perkin Trans. 1* **1975**, 591−593.
(37) House, D. A.; Hay, R. W.; Ali, M. A. The Preparation and Characterization of Chromium(III) Complexes of C-Meso and C-Racemic-5,7,7,12,14,14-Hexamethyl-1,4,8,11-Tetraazacyclotetradecane (Tet-a and Tet-B). *Inorg. Chim. Acta* **1983**, *72*, 239−245.
(38) Lubbecke, H.; Boldt, P. Quinones 0.7. Halogenation and Oxidative Halogenation of Phenols with Hydrogen Halides and Hydrogen Peroxide - Synthesis of Para-Chloranil and Para-Bromanil. *Tetrahedron* **1978**, *34*, 1577−1579.
(39) Bruker, 2016. Apex3 v2016.9-0, Saint V8.34A, SAINT V8.37A, Bruker AXS Inc.: Madison, WI, 2013/2014, 2016.
(40) (a) SHELXTL suite of programs Version 6.14. Bruker Advanced X-ray Solutions, Bruker AXS Inc., Madison, WI, 2000−2003. (b) Sheldrick, G. M. A short history of SHELX. *Acta Crystallogr., Sect. A: Found. Crystallogr.* **2008**, *64*, 112−122.
(41) Frisch, M. J.; Trucks, G. W.; Schlegel, H. B.; Scuseria, G. E.; Robb, M. A.; Cheeseman, J. R.; Scalmani, G.; Barone, V.; Petersson, G. A.; Nakatsuji, H.; Li, X.; Caricato, M.; Marenich, A. V.; Bloino, J.; Janesko, B. G.; Gomperts, R.; Mennucci, B.; Hratchian, H. P.; Ortiz, J. V.; Izmaylov, A. F.; Sonnenberg, J. L.; Williams-Young, D.; Ding, F.; Lipparini, F.; Egidi, F.; Goings, J.; Peng, B.; Petrone, A.; Henderson, T.; Ranasinghe, D.; Zakrzewski, V. G.; Gao, J.; Rega, N.; Zheng, G.; Liang, W.; Hada, M.; Ehara, M.; Toyota, K.; Fukuda, R.; Hasegawa, J.; Ishida, M.; Nakajima, T.; Honda, Y.; Kitao, O.; Nakai, H.; Vreven, T.; Throssell, K.; Montgomery, J. J. A.; Peralta, J. E.; Ogliaro, F.; Bearpark, M. J.; Heyd, J. J.; Brothers, E. N.; Kudin, K. N.; Staroverov, V. N.; Keith, T. A.; Kobayashi, R.; Normand, J.; Raghavachari, K.; Rendell, A. P.; Burant, J. C.; Iyengar, S. S.; Tomasi, J.; Cossi, M.; Millam, J. M.; Klene, M.; Adamo, C.; Cammi, R.; Ochterski, J. W.; Martin, R. L.; Morokuma, K.; Farkas, O.; Foresman, J. B.; Fox, D. J. *Gaussian 16, Rev. A.03*.
(42) Zhao, Y.; Truhlar, D. G. The M06 suite of density functionals for main group thermochemistry, thermochemical kinetics, noncovalent interactions, excited states, and transition elements: two new functionals and systematic testing of four M06-class functionals and 12 other functionals. *Theor. Chem. Acc.* **2008**, *120*, 215−241.
(43) Weigend, F.; Ahlrichs, R. Balanced basis sets of split valence, triple zeta valence and quadruple zeta valence quality for H to Rn: Design and assessment of accuracy. *Phys. Chem. Chem. Phys.* **2005**, *7*, 3297−3305.
(44) Grimme, S.; Antony, J.; Ehrlich, S.; Krieg, H. A consistent and accurate ab initio parametrization of density functional dispersion correction (DFT-D) for the 94 elements H-Pu. *J. Chem. Phys.* **2010**, *132*, 154104.
(45) Cossi, M.; Rega, N.; Scalmani, G.; Barone, V. Energies, structures, and electronic properties of molecules in solution with the C-PCM solvation model. *J. Comput. Chem.* **2003**, *24*, 669−681.

https://dx.doi.org/10.1021/acs.inorgchem.0c03224
Inorg. Chem. 2021, 60, 4447−4455